frontiers | Frontiers in Artificial Intelligence

TYPE Original Research
PUBLISHED 12 January 2026
DOI 10.3389/frai.2025.1702056

OPEN ACCESS

EDITED BY
Andrejs Romanovs,
Riga Technical University, Latvia

REVIEWED BY
Wei Ren,
Xi'an University of Posts and Telecommunications, China
Duorui Gao,
Chinese Academy of Sciences (CAS), China
Jawad Mirza,
HITEC University, Pakistan

*CORRESPONDENCE
Zhiyuan Wang
✉ wzy01930@mails.guet.edu.cn

RECEIVED 09 September 2025
REVISED 27 November 2025
ACCEPTED 10 December 2025
PUBLISHED 12 January 2026

CITATION
Li X and Wang Z (2026) Physics-constrained GAN boosts OAM correction in ocean turbulence. *Front. Artif. Intell.* 8:1702056. doi: 10.3389/frai.2025.1702056

Physics-constrained GAN boosts OAM correction in ocean turbulence

Xiaoji Li and Zhiyuan Wang*

Key Laboratory of Cognitive Radio and Information Processing, Ministry of Education, Guilin University of Electronic Technology, Guilin, China

Introduction: This study addresses the challenge of improving wavefront correction for Orbital Angular Momentum (OAM) in oceanic turbulence using a physics-constrained Generative Adversarial Network (GAN).
Methods: We integrated physical constraints into a deep learning framework to reconstruct degraded input images (SSIM = 0.62). The model was trained with varied loss settings, including a baseline model, spectral constraints (+Spec), and spatial constraints (+Ortho).
Results: The dual-constraint approach (+Ortho+Spec) reached a near-optimal SSIM of 0.98. Ablation studies revealed that while +Ortho boosted modal purity to 95.7%, the dual-constraints achieved 98.4% purity. Power spectral density analysis via KL divergence confirmed the dual-constraints' superiority (KL = 0.56) over the baseline (KL = 2.47).
Discussion: These results demonstrate that integrating both spatial and spectral constraints effectively optimizes reconstruction, purity, and spectral fidelity, offering a robust solution for OAM correction in underwater optical communication systems.

KEYWORDS

machine learning, physics-constrained GAN, OAM, oceanic turbulence correction, underwater optical communication

1 Introduction

Underwater optical wireless communication (UOWC) systems have emerged as a promising technology for high-bandwidth data transmission, yet they face fundamental limitations due to the complex nature of the oceanic channel (Vali et al., 2025; Baykal et al., 2022). Among the various multiplexing techniques, Orbital Angular Momentum (OAM) beams are particularly valuable for increasing channel capacity, as their helical phase fronts carry distinct topological charges that serve as independent information carriers (Wang and Willner, 2014; Guo et al., 2023). However, the reliability of OAM-based links is severely compromised by oceanic turbulence, which induces complex inhomogeneities in the propagation medium.

It is crucial to distinguish the specific impact of wavefront distortions from general intensity fluctuations in OAM systems. While oceanic turbulence manifests as both scintillation (intensity fluctuation) and phase aberrations, their effects on signal integrity differ fundamentally. Intensity fluctuations primarily degrade the Signal-to-Noise Ratio (SNR), leading to signal fading. In contrast, wavefront distortions directly perturb the helical phase structure that defines OAM modes. This phase disruption destroys the orthogonality between modes,

inducing severe inter-modal cross-talk that cannot be resolved by simple intensity smoothing. Therefore, restoring the wavefront's structural integrity—specifically the phase singularity—is a prerequisite for recovering the channel capacity, necessitating correction strategies that go beyond mere image denoising (Subramaniam et al., 2020).

In response to these challenges, the integration of Machine Learning (ML) and Deep Learning (DL) into optical communication systems has evolved significantly in recent years. A comprehensive survey by Amirabadi et al. highlights the growing reliance on these data-driven techniques for channel modeling and signal processing (Amirabadi et al., 2024). In the realm of UOWC, Deep Reinforcement Learning (DRL) has emerged as a powerful tool for system optimization. For instance, Rathour utilized DRL to enhance link performance in dynamic underwater environments (Rathour, 2023), while Shin et al. applied similar strategies for multidimensional beam optimization (Shin et al., 2024). Complementing these adaptive approaches, Simon et al. proposed energy-adaptive neural networks to improve efficiency in underwater IoT networks (Simon et al., 2025), and Shafi et al. explored spatial diversity techniques to mitigate oceanic channel impairments (Shafi et al., 2025). Beyond system-level optimization, DL architectures have been successfully deployed to improve signal integrity, with Iqbal et al. demonstrating significant reductions in symbol error rates for short-reach optical networks (Iqbal et al., 2024). Regarding OAM systems specifically, Ye et al. developed hybrid optical-electronic Convolutional Neural Networks (CNNs) for efficient OAM demultiplexing (Ye et al., 2024), and Cai et al. achieved accurate recognition of composite vortex beams even under moderate-to-strong turbulence (Cai et al., 2024). To address turbulence-induced distortions, recent studies have advanced from general underwater image enhancement (Liu, 2025) to precise wavefront reconstruction. Baharlou et al. introduced hybrid networks for single-shot aberration correction (Baharlou et al., 2025), while Zhang et al. utilized neural operators for depth-heterogeneous turbulence correction (Zhang et al., 2025). Notably, Long et al. demonstrated that physics-informed neural networks could achieve in situ wavefront correction, validating the efficacy of combining data-driven learning with physical laws (Long et al., 2024).

Despite these advancements, generative models, particularly Generative Adversarial Networks (GANs), which treat wavefront correction as an image-to-image translation task, often show potential but face limitations (Pradhyumna and Mohana, 2022). Models like pix2pix map distorted intensity profiles to their ideal counterparts (Isola et al., 2016). However, these conventional implementations frequently overlook the inherent physical laws governing light-turbulence interactions (Newman et al., 2011). By relying predominantly on pixel-wise loss functions (e.g., L1 or L2 norms), standard GANs tend to optimize visual similarity (intensity restoration) while neglecting the preservation of topological charge integrity and spectral dynamics (Zhan et al., 2021).

This oversight results in two critical deficiencies in current methods. First, the reconstructed beams often exhibit reduced mode orthogonality due to residual phase errors, limiting the achievable channel separation (Wulff et al., 2023; Zhang et al., 2024). Second, the generated turbulence compensation often fails to align with the theoretical Power Spectral Density (PSD) of oceanic turbulence (e.g., von Kármán model), leading to poor generalization under non-stationary scattering conditions. Although isolated constraints, such as spatial orthogonality (+Ortho) or spectral regularization (+Spec), have been explored, their separate application fails to capture the synergistic physical interdependencies required for robust correction.

To address these challenges, this study proposes a physics-constrained GAN framework that systematically optimizes OAM wavefront correction. By integrating a dual-constraint mechanism—combining spatial orthogonality priors with spectral compliance regularization—into the pix2pix architecture, we bridge the gap between data-driven image generation and optical physics. Our approach not only achieves superior reconstruction fidelity (SSIM = 0.98) but, more importantly, restores modal purity to near-optimal levels (98.4%) and ensures strict adherence to Kolmogorov turbulence statistics. This unified framework offers a robust solution for maintaining high-capacity OAM communications in turbulent marine environments.

2 Methods

As illustrated in Figure 1, the OAM transmission system schematic comprises three functional modules: (1) OAM beam generation, (2) turbulent oceanic propagation channel, and (3) receiver-side wavefront correction. The workflow demonstrates MATLAB-simulated OAM intensity profiles undergoing distortion through the marine turbulence channel, followed by image reconstruction via the physics-constrained GAN correction model.

2.1 Fundamentals of Laguerre–Gaussian (LG) beams

LG beates. In cylindrical coordinates, the LG beam propagating along the z-axis can be expressed as:

$$\begin{aligned} LG_p^L(r,\theta,z) &= \frac{c}{\sqrt{1+z^2/z_R^2}}\left[\frac{r\sqrt{2}}{\omega(z)}\right]^{|L|} L_p^L\left[\frac{2r^2}{\omega^2(z)}\right] \\ &\exp\left[\frac{-r^2}{\omega^2(z)}\right]\times\exp\left[\frac{ikr^2z}{2(z^2+z_R^2)}\right]\times\exp(iL\theta) \\ &\exp[-i(2p+L+1)arctan\frac{z}{z_R}] \end{aligned} \quad (1)$$

where p denotes the radial mode index governing concentric intensity nodes, L represents the topological charge generating helical wavefronts and orbital angular momentum hL per photon, $\omega(z) \equiv \omega_0\sqrt{1+(z/z_R)^2}$ defines the z-dependent beam radius, with ω_0 being the waist size, $z_R = \pi\omega_0^2/\lambda$ is the Rayleigh range characterizing focal confinement, $k = 2\pi/\lambda$ encodes the wavelength λ, and $L_p^L(\cdot)$ specifies the radial intensity profile via associated Laguerre polynomials. The phase structure includes wavefront curvature $\exp[ikr^2z/(2(z^2+z_R^2))]$, azimuthal

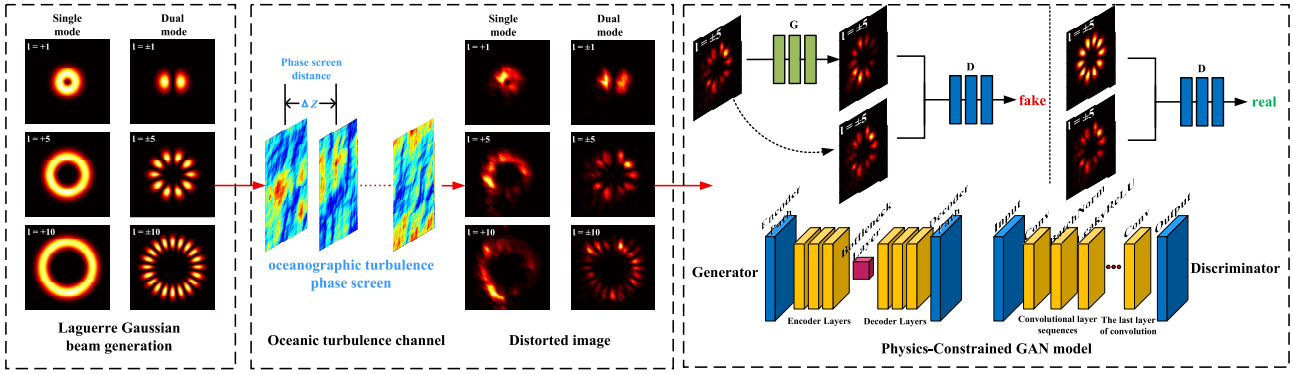

FIGURE 1
OAM transmission and correction system in an oceanic turbulence channel.

phase singularity $\exp(iL\theta)$, and mode-order-dependent Gouy shift $\exp[-i(2p + |L| + 1)\tan^{-1}(z/z_R)]$, collectively sustaining the characteristic doughnut-shaped intensity and OAM-carrying properties under paraxial propagation (Allen et al., 1992; Miyamoto, 2004).

2.2 Limitations of the standard Pix2pix framework

GANs integrate two neural networks—the Generator (G) and Discriminator (D)—that undergo adversarial training to iteratively optimize their performance (Goodfellow et al., 2020; Sun, 2025). The generator synthesizes realistic outputs from random noise or degraded inputs. Within underwater optical communication systems, where OAM modes suffer from marine turbulence-induced distortion, the generator processes turbulence-distorted OAM data (e.g., light-field images) and learns to reconstruct distortion-free or minimally distorted representations. Concurrently, the discriminator evaluates whether inputs derive from authentic, distortion-free datasets or are synthetic outputs from the generator, assigning a probability score to quantify the likelihood of authenticity.

Pix2pix, a conditional GAN variant, specializes in image-to-image translation (Lin, 2023). For OAM turbulence correction, this framework maps distorted light-field images to their undistorted equivalents, minimizing a composite loss function:

$$L_{pix2pix} = E_{x,y}[logD(x,y)] + E_x[log(1 - D(x,G(x)))] + \lambda||y - G(x)||_1 \quad (2)$$

where G denotes the generator and D the discriminator. Critically, this framework suffers from three physical oversights:

(i) Spatial non-orthogonality: The pixel-wise L_1 loss disregards the orthogonality of OAM modes, permitting residual modal interference in reconstructions.

(ii) Spectral misalignment: Turbulence-induced PSD distortions deviate from the theoretical von Kármán spectrum, lacking spectral-physical regularization.

(iii) Physics-agnostic optimization: Training fails to incorporate known light-turbulence interaction physics, limiting generalizability under non-stationary scattering conditions.

2.3 Proposed dual-constraint GAN architecture

To address the limitations of conventional pix2pix in LG beam reconstruction, we propose a physics-constrained GAN framework. As illustrated in Figure 2, this architecture integrates dual-domain physical priors into the adversarial training process through three interconnected phases: reconstruction, physics-constraint embedding, and optimization. In the reconstruction phase, the generator G (based on a U-Net architecture, see Table 1 for details) synthesizes a corrected wavefront $G(x)$ from the turbulence-distorted input x. To ensure physical fidelity, we incorporate spatial orthogonality and spectral compliance constraints into the unified optimization objective L_{dual}, formulated as:

$$L_{dual} = E_{x,y}[logD(x,y)] + E_x[log(1 - D(x,G(x)))] + \lambda||y - G(x)||_1 + \alpha L_{Ortho} + \beta L_{Spec} \quad (3)$$

where the first two terms represent the adversarial loss, the third term is the $L1$ reconstruction loss, and L_{Ortho} and L_{Spec} represent the physical constraints weighted by hyperparameters α and β (detailed settings provided in Table 1).

Crucially, the "embedding logic" of these physical constraints is operationalized through parallel validation branches, as depicted in the physics-constraint phase of Figure 2. In the spatial domain, the spatial orthogonality loss (L_{Ortho}) enforces mode separation by minimizing inter-modal cross-talk, calculated via the overlap integral over the beam cross-section Ω:

$$L_{Ortho} = \sum_p \sum_{\ell \neq \ell'} \iint_\Omega u^*_{p,\ell}(r,\phi) u_{p,\ell'}(r,\phi) r dr d\phi|^2 \quad (4)$$

where ideally, the integral approaches zero for orthogonal LG modes ($u_{p,l}$). Simultaneously, in the frequency domain, the

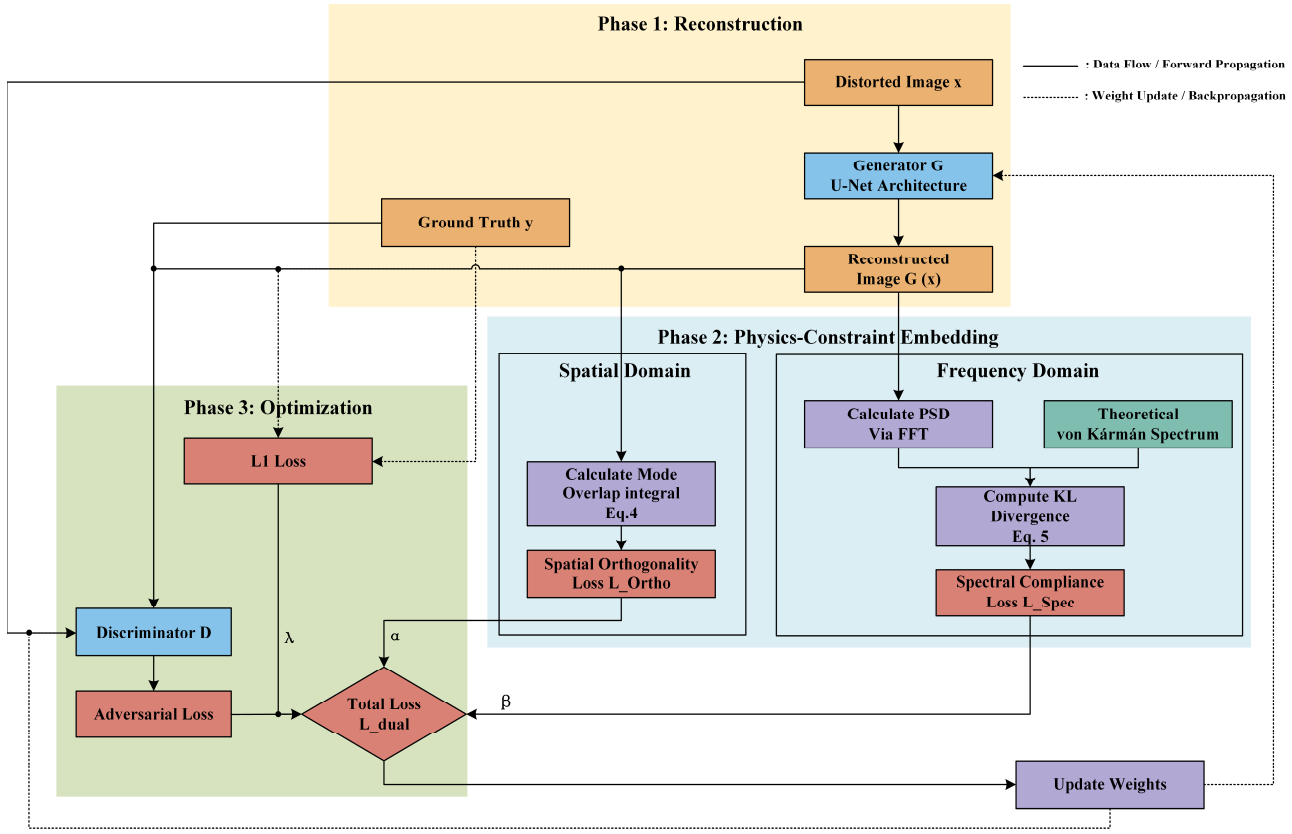

FIGURE 2
Schematic diagram of the proposed physics-constrained GAN architecture, illustrating the data flow across reconstruction, physics-constraint, and optimization phases.

spectral alignment loss (L_{Spec}) regularizes turbulence statistics by minimizing the KL divergence between the generated image's PSD, $S_G(f)$, and the theoretical von Kármán spectrum, $S_{vK}(f)$:

$$L_{Spec} = D_{KL}(S_G(f) \parallel S_{vK}(f)) = \int_{-\infty}^{\infty} S_G(f) log \frac{S_G(f)}{S_{vK}(f)} df \quad (5)$$

During the final optimization phase, gradients derived from these physical constraints are aggregated with adversarial and reconstruction gradients and backpropagated to update the generator. This mechanism ensures that the model learns to correct wavefronts that are not only visually consistent with the ground truth but also rigorously adhere to the underlying physics of optical propagation.

3 Numerical results and discussions

3.1 Simulation data set construction

Selecting a suitable and relevant channel model is fundamental to evaluating the performance of Underwater Optical Wireless Communication (UWOC) systems, as it determines the accuracy of signal degradation simulation under realistic conditions. Various statistical models have been proposed to characterize fading in Free Space Optical (FSO) and UWOC links, including the log–normal distribution for weak turbulence and the gamma–gamma distribution for moderate-to-strong turbulence regimes (Armghan et al., 2025). However, while these statistical models effectively describe intensity fluctuations (scintillation), OAM-based systems require a spatially resolved representation of wavefront phase distortions. Therefore, employing a phase-screen model based on the power spectral density of refractive index fluctuations is essential to capture the spatial structure of turbulence-induced aberrations.

To rigorously evaluate the performance of the physics-constrained pix2pix, we constructed two complementary OAM datasets simulating varying oceanic turbulence conditions. All optical fields were synthesized in MATLAB using a unified paraxial split-step beam propagation method.

3.1.1 Beam and propagation parameters

The simulation setup utilized a square aperture of [-3, 3] cm sampled on a 512×512 grid. We generated zero-radial-order LG beams ($p = 0$) with a waist radius of $\omega_0 = 5$ mm at a wavelength of $\lambda = 532\ nm$. The beams were propagated over a distance of $Z_0 = 80$ m, divided into 10 steps, with an independent phase screen applied at each step to simulate the cumulative effect of continuous turbulence.

TABLE 1 Detailed implementation specifications and hyperparameter settings of the proposed physics-constrained GAN.

Category	Parameter	Value/description
Architecture	Generator structure	U-Net (encoder-decoder with skip connections)
	Generator depth	15 Convolutional blocks (8 encoder, 7 decoder)
	Discriminator structure	PatchGAN (70 × 70 receptive field)
	Activation functions	LeakyReLU (slope = 0.2) for encoder/discriminator; ReLU for decoder
	Normalization	Batch normalization
	Input/output resolution	512 × 512 pixels
Training	Optimizer	Adam (β1 = 0.5, β2 = 0.999)
	Learning rate	0.0002 (constant for first 50 epochs, linear decay to 0)
	Batch size	1
	Total epochs	100
Loss Weights	Adversarial loss weight	1
	L1 Reconstruction weight (λ)	100.0
	Spatial orthogonality weight (α)	0.5
	Spectral compliance weight (β)	0.3

3.1.2 Oceanic turbulence channel model

To ensure physical consistency with real-world marine environments, the phase screens were generated based on the classic Nikishov–Khmenko (NK) power spectrum model of refractive-index fluctuations. This model characterizes the turbulence PSD, $\Phi_n(\kappa)$, incorporating the contributions of both temperature and salinity fluctuations (Nikishov and Nikishov, 2000; Mirza et al., 2025):

$$\Phi_n(\kappa) = 0.388 \times 10^{-8}\varepsilon^{-1/3}\kappa^{-11/3}\frac{\chi_T}{\omega^2} \times (A_T e^{-A_T\delta} + A_S e^{-A_S\delta} + A_{TS}e^{-A_{TS}\delta} \quad (6)$$

where ε is the rate of dissipation of kinetic energy and χ_T is the dissipation rate of mean-squared temperature. The specific coefficients for the spectral terms were selected based on standard empirical values for seawater reported in Nikishov and Khmenko's foundational studies: $A_T = 1.863 \times 10^{-2}$, $A_S = 1.9 \times 10^{-4}$, and $A_{TS} = 9.41 \times 10^{-3}$ (with $\omega = -2$). The scalar dissipation was set to $\varepsilon = 10^{-4} m^2/s^3$.

To validate the model's robustness across diverse oceanographic conditions, we varied the refractive-index structure constant ($C_n^2 = 10^{-8}\chi_T\varepsilon^{-1/3}$) by adjusting χ_T to create three representative regimes:

(i) Weak turbulence: $C_n^2 = 10^{-15}m^{-2/3}$.

(ii) Moderate turbulence: $C_n^2 = 10^{-14}m^{-2/3}$.

(iii) Strong turbulence: $C_n^2 = 10^{-13}m^{-2/3}$.

This parameter space ensures that the generated datasets cover the majority of signal degradation scenarios encountered in practical underwater optical communications (Du et al., 2023).

3.1.3 Dataset composition

For each turbulence regime defined above, we generated two distinct datasets to comprehensively evaluate the model's reconstruction capabilities:

(i) Single-mode subset (10 classes): This subset consists of single-aperture LG beams with topological charges ranging from $|l| = 1$ to $|l| = 10$. It serves as the baseline for evaluating the restoration of fundamental OAM modes.

(ii) Superposition subset (10 classes): This subset comprises coherent superpositions of conjugate OAM pairs (i.e., combining $+l$, and $-l$ modes) for $l = 1 \ldots 10$. These composite modes feature complex petal-like intensity structures, providing a more challenging test for spatial reconstruction.

3.2 Analysis of OAM wavefront correction results based on physics-constrained GAN

To quantitatively assess the restoration fidelity, we reconstructed turbulence-degraded images (initial SSIM = 0.62) using distinct loss configurations, as illustrated in Figure 3 and summarized in Table 2. The baseline model, driven solely by standard pix2pix loss, improved the SSIM to 0.84 but failed to fully resolve the beam's fine structure. Introducing the spectral constraint (+Spec) yielded a marginal improvement (SSIM = 0.86), whereas the spatial constraint (+Ortho) significantly elevated the SSIM to 0.95.

Critically, the dual-constraint architecture (+Ortho+Spec) achieved a near-optimal SSIM of 0.98. This performance leap stems from the synergistic interaction of the constraints: the spatial term (L_{Ortho}) restores the distinct topological structure of the OAM modes by penalizing geometric distortions, while the spectral term (L_{Spec}) suppresses non-physical high-frequency artifacts. This ensures the reconstruction is not only visually sharp but physically consistent with the propagation properties of LG beams.

The ablation study in Figure 4 isolates the impact of physical constraints on OAM mode purity. The baseline model yielded a purity of 85.0%. Incorporating the spatial constraint (+Ortho) resulted in the most significant single-factor gain, boosting purity by 10.7% to 95.7%, whereas the frequency constraint (+Spec) provided a modest increase of 1.5% (to 86.5%).

The dual-constraint framework achieved a peak purity of 98.4%, representing a 13.4% absolute improvement over the baseline. Physically, this validates the necessity of the orthogonality constraint (L_{Ortho}), which explicitly acts as a regularizer against modal cross-talk. By minimizing the overlap integral between different modes during training, the network learns to "unmix" the turbulence-induced energy leakage, thereby preserving the

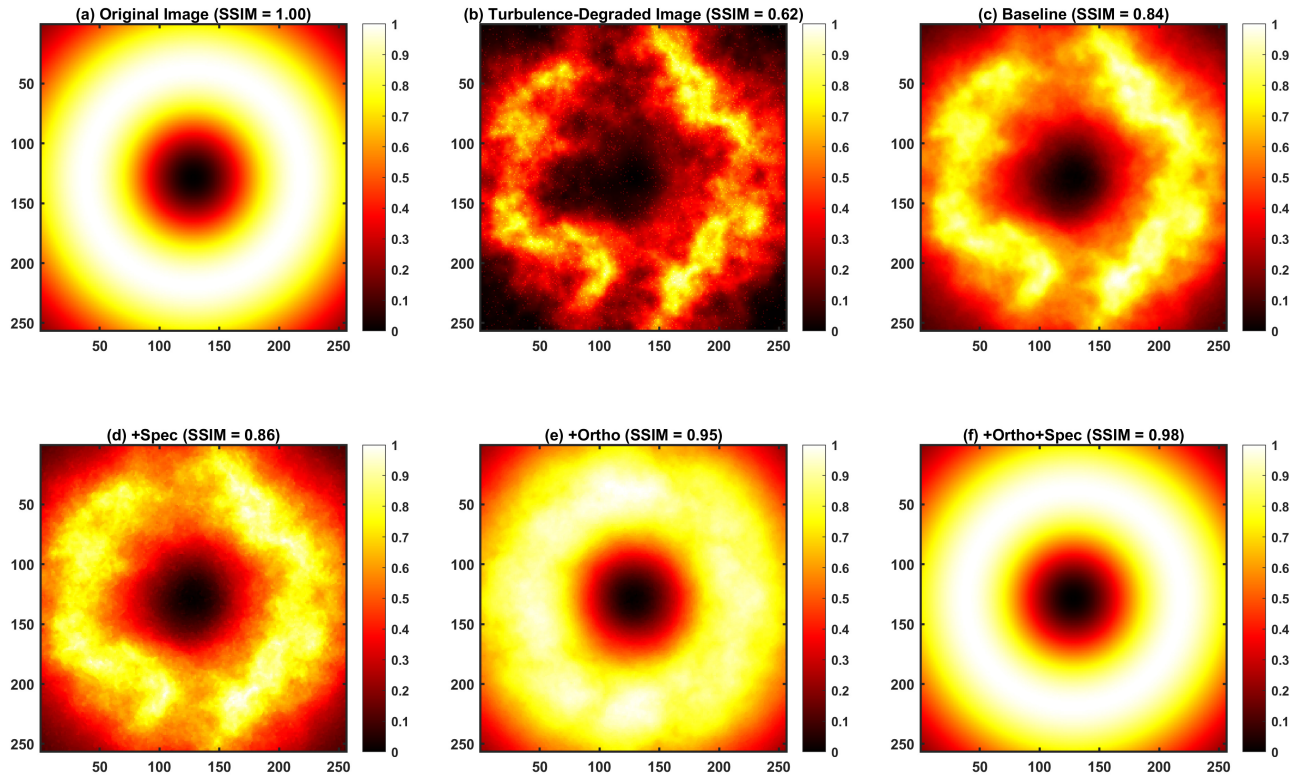

FIGURE 3
Comparative analysis of OAM wavefront correction using physically-constrained pix2pix under oceanic turbulence with SSIM evaluation. **(a)** Original Image (undistorted reference); **(b)** Turbulence-Degraded Image (initial degraded state); **(c)** Baseline (original pix2pix loss, no physical constraints); **(d)** +Spec (baseline + turbulence spectrum KL divergence, spectral constraints only); **(e)** +Ortho (baseline + phase orthogonality loss, spatial constraints only); **(f)** +Ortho+Spec (baseline + dual constraints, spatial and spectral joint constraints).

TABLE 2 Comparison of SSIM values for different processing methods.

Subfigure	Description	SSIM value
(a)	Original image (undistorted reference)	1.00
(b)	Turbulence-degraded image (initial degraded state)	0.62
(c)	Baseline (original pix2pix loss, no physical constraints)	0.84
(d)	+Spec (baseline + turbulence spectrum KL divergence, spectral constraints only)	0.86
(e)	+Ortho (baseline + phase orthogonality loss, spatial constraints only)	0.95
(f)	+Ortho+Spec (baseline + dual constraints, spatial and spectral joint constraints)	0.98

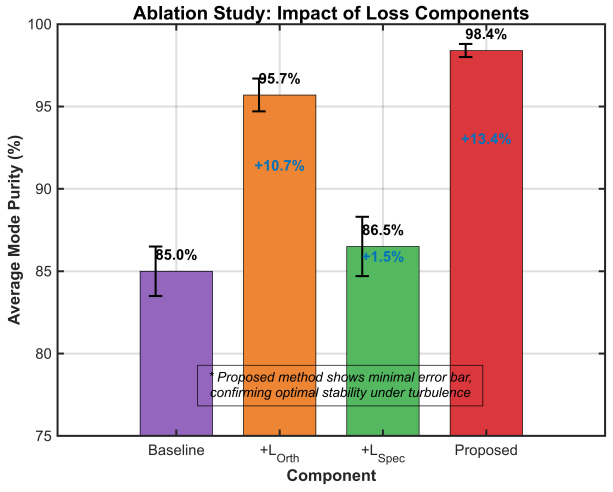

FIGURE 4
Ablation study impact of loss components.

wavefront's phase singularity and topological charge integrity even under severe distortion.

To verify whether the generated images adhere to oceanic turbulence statistics, we analyzed the PSD alignment using KL divergence, as shown in Figure 5. The baseline model exhibited a high divergence (KL = 2.47), indicating a spectral mismatch where the network hallucinated artificial high-frequency texture to mimic sharpness.

In contrast, the dual-constraint model minimized the KL divergence to 0.56, achieving the closest alignment with the theoretical von Kármán spectrum. This demonstrates that the spectral loss (L_{Spec}) effectively constrains the generator to replicate the statistical distribution of the theoretical von Kármán spectrum. By aligning the output with the characteristic energy decay of the inertial subrange, the model prevents the generation of "spatially

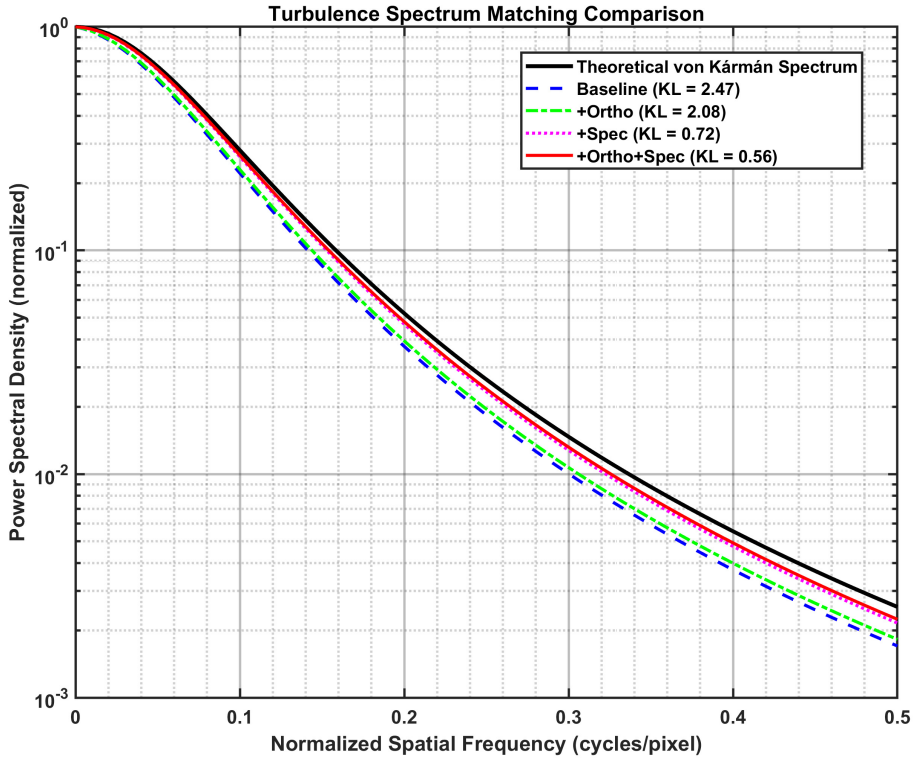

FIGURE 5
Turbulence spectrum matching comparison.

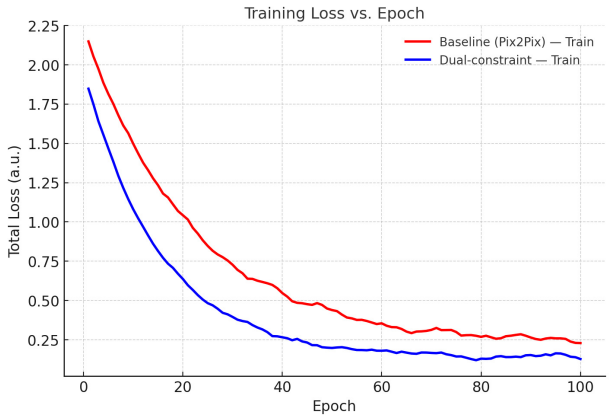

FIGURE 6
Training loss vs. epoch (total loss).

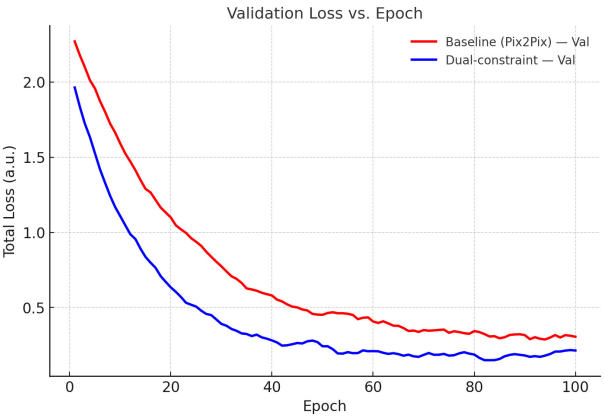

FIGURE 7
Validation loss vs. epoch (total loss).

clear but physically erroneous" features, ensuring high spectral fidelity essential for stable beam propagation.

To assess the influence of physical constraints on OAM wavefront correction in oceanic turbulence, we analyzed the loss trajectories of the unconstrained baseline pix2pix model and the dual spatial-frequency constrained model across training and validation sets. As depicted in Figure 6 (training loss vs. epoch), the dual-constrained model achieved a lower initial loss (1.83 vs. 2.14 at epoch 0) and demonstrated accelerated convergence, with the final loss being markedly reduced compared to the baseline model. Furthermore, Figure 7 (validation loss vs. epoch) reveals that the dual-constrained model maintained a superior performance advantage throughout the training process, notably exhibiting a loss of 0.3 vs. 0.6 at epoch 40 and culminating in a lower final validation loss at epoch 100. These results indicate that the dual constraints effectively enhance training dynamics and generalization capability, ultimately leading to more robust validation performance.

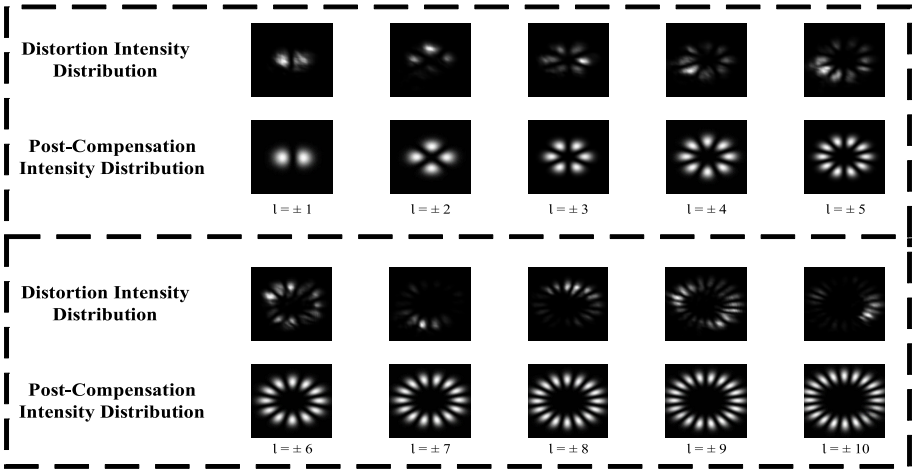

FIGURE 8
Intensity distributions of distorted and compensated OAM beams with topological charges $l = \pm 1$ to $l = \pm 10$.

Finally, to comprehensively verify the performance of the physics-constrained GAN, we examined the intensity profiles of OAM beams spanning topological charges $l = \pm 1$ to $l = \pm 10$ under oceanic turbulence conditions ($C_n^2 = 10^{-13}, \omega = -2$). In the distorted state, all modes displayed pronounced deformation and loss of symmetry, reflecting significant turbulence-induced cross-talk. Following compensation, the beams recovered their characteristic ring-shaped structures, with clear enhancements in modal definition and orthogonality. As illustrated in Figure 8, higher-order modes ($l = \pm 6$ to $l = \pm 10$) exhibited substantial restoration of structural fidelity, underscoring the model's ability to maintain mode purity under severe turbulence. Taken together, this final evidence confirms that incorporating dual spatial–spectral constraints ensures robust OAM correction across diverse modes, thereby enabling reliable transmission in turbulent oceanic environments.

4 Conclusions

Employing the pix2pix framework, we quantified the impact of physics priors on correcting OAM wavefront distortions in oceanic turbulence. From degraded inputs (SSIM = 0.62), the baseline model improved the SSIM to 0.84. A spectral KL constraint (+Spec) marginally increased SSIM to 0.86 while strongly aligning the output spectrum with the von Kármán model (KL 2.47→ 0.72; −70.9%). In contrast, a spatial phase-orthogonality constraint (+Ortho) yielded substantial gains in structural fidelity (SSIM = 0.95; +0.11 over baseline) and mode purity (85.0%→ 95.7%; +10.7 pp), while offering only a modest spectral reduction (KL 2.47→ 2.08; −15.8%). The joint model (+Ortho+Spec) achieved the best overall performance: SSIM = 0.98 (near 1.00), the lowest spectral discrepancy (KL = 0.56; −77.3%), and the highest OAM purity (98.4%; +13.4 pp). These ablations indicate that single-domain priors are helpful but incomplete (+Spec raises purity only to 86.5%; +1.5 pp), whereas coupling spatial and spectral constraints creates a holistic physics prior that simultaneously preserves OAM modal structure and enforces turbulence statistics. Training dynamics corroborate this synergy, showing faster stabilization and consistently lower losses than the baseline on both training and validation sets.

Data availability statement

The raw data supporting the conclusions of this article will be made available by the authors, without undue reservation.

Author contributions

XL: Funding acquisition, Methodology, Project administration, Writing – review & editing. ZW: Data curation, Investigation, Software, Validation, Visualization, Writing – original draft.

Funding

The author(s) declared that financial support was received for this work and/or its publication. This research was funded by Guangxi Natural Science Foundation of General Project (2025GXNSFAA069513); Guangxi Education Department Key Project of Educational Reform (No. 2024JGZ127); and Cognitive Radio and Information Processing Provincial-Ministry Joint Key Laboratory of the Ministry of Education Open Fund Project (No. CRKL210103).

Conflict of interest

The author(s) declared that this work was conducted in the absence of any commercial or financial relationships that could be construed as a potential conflict of interest.

Generative AI statement

The author(s) declared that generative AI was not used in the creation of this manuscript.

Any alternative text (alt text) provided alongside figures in this article has been generated by Frontiers with the support of artificial intelligence and reasonable efforts have been made to ensure accuracy, including review by the authors wherever possible. If you identify any issues, please contact us.

Publisher's note

References

Allen, L., Beijersbergen, M. W., Spreeuw, R. J. C., and Woerdman, J. P. (1992). Orbital angular momentum of light and the transformation of Laguerre-Gaussian laser modes. *Phys. Rev. A* 45, 8185–8189. doi: 10.1103/PhysRevA.45.8185

Amirabadi, M. A., Nezamalhosseini, S. A., Kahaei, M. H., and Chen, L. R. (2024). A survey on machine and deep learning for optical communications (version 1). *arXiv*. doi: 10.48550/arXiv.2412.17826

Armghan, A., Alsharari, M., Aliqab, K., Alrashdi, I., Kanwal, B., Mirza, J., et al. (2025). High-speed and potentially scalable UWOC/UWB converged transmission link for underwater wireless optical sensor networks. *Front. Phys.* 13:1650284. doi: 10.3389/fphy.2025.1650284

Baharlou, S. M., Khalid, M. W., Sergienko, A. V., and Ndao, A. (2025). "Single-shot wavefront aberration correction using a hybrid neural network approach," in *CLEO 2025, SS118_7* (Washington, DC: Optica Publishing Group). doi: 10.1364/CLEO_SI.2025.SS118_7

Baykal, Y., Ata, Y., and Gökçe, M. C. (2022). Underwater turbulence, its effects on optical wireless communication and imaging: a review. *Optics Laser Technol.* 156:108624. doi: 10.1016/j.optlastec.2022.108624

Cai, S., Li, Z., Zhong, Z., and Zhang, B. (2024). Deep-learning-based recognition of composite vortex beams through long-distance and moderate-to-strong atmospheric turbulence. *Phys. Rev. A* 110:013508. doi: 10.1103/PhysRevA.110.013508

Du, Z., Ge, W., Cai, C., Wang, H., Song, G., and Shen, C. (2023). 90-m/660-Mbps underwater wireless optical communication enabled by interleaved single-carrier FDM scheme combined with sparse weight-initiated DNN equalizer. *J. Lightwave Technol.* 41, 5310–5320. doi: 10.1109/JLT.2023.3262352

Goodfellow, I., Pouget-Abadie, J., Mirza, M., Xu, B., Warde-Farley, D., Ozair, S., et al. (2020). Generative adversarial networks. *Commun. ACM* 63, 139–144. doi: 10.1145/3422622

Guo, Y., Li, L., Wang, J., Gao, C., and Fu, S. (2023). Distortion compensation for orbital angular momentum beams: from probing to deep learning. *J. Lightwave Technol.* 41, 2041–2050. doi: 10.1109/JLT.2022.3218828

Iqbal, M., Ghafoor, S., Ahmad, A., Aljohani, A. J., Mirza, J., Aziz, I., et al. (2024). Symbol error rate minimization using deep learning approaches for short-reach optical communication networks. *Front. Phys.* 12:1387284. doi: 10.3389/fphy.2024.1387284

Isola, P., Zhu, J.-Y., Zhou, T., and Efros, A. A. (2016). "Image-to-image translation with conditional adversarial networks (version 3)," in *2017 IEEE Conference on Computer Vision and Pattern Recognition (CVPR)*, 1125–1134. doi: 10.1109/CVPR.2017.632

Lin, E. (2023). Comparative analysis of Pix2Pix and CycleGAN for image-to-image translation. *Highlights Sci. Eng. Technol.* 39, 915–925. doi: 10.54097/hset.v39i.6676

Liu, X. (2025). "Research on machine learning-based underwater image enhancement methods under multi-module fusion modeling," in*2025 IEEE 5th International Conference on Electronic Technology, Communication and Information (ICETCI)* (Piscataway, NJ: IEEE), 980–986. doi: 10.1109/ICETCI64844.2025.11084007

Long, X., Gao, Y., Yuan, Z., Yan, W., Ren, Z., Wang, X., et al. (2024). *In-situ* wavefront correction via physics-informed neural network. *Laser Photon. Rev.* 18:833. doi: 10.1002/lpor.202300833

Mirza, J., Atieh, A., Kanwal, B., and Ghafoor, S. (2025). Relay aided UWOC-SMF-FSO based hybrid link for underwater wireless optical sensor network. *Optical Fiber Technol.* 89:104045. doi: 10.1016/j.yofte.2024.104045

Miyamoto, Y. (2004). Laguerre-gaussian beams and optical orbital angular momentum. *Rev. Laser Eng.* 32, 232–236. doi: 10.2184/lsj.32.232

Newman, J. A., Wang, Z., and Webb, K. J. (2011). "Incident field image reconstruction using speckle intensity correlations over position," in *CLEO:2011 - Laser Applications to Photonic Applications, CMG4* (Washington, DC: Optica Publishing Group). doi: 10.1364/CLEO_SI.2011.CMG4

Nikishov, V. V., and Nikishov, V. I. (2000). Spectrum of turbulent fluctuations of the sea-water refraction index. *Int. J. Fluid Mech. Res.* 27, 82–98. doi: 10.1615/InterJFluidMechRes.v27.i1.70

Pradhyumna, P., and Mohana. (2022). "A survey of modern deep learning based generative adversarial networks (GANs)," in *2022 6th International Conference on Computing Methodologies and Communication (ICCMC)* (Piscataway, NJ: IEEE), 1146–1152. doi: 10.1109/ICCMC53470.2022.9753782

Rathour, A. (2023). "Performance enhancement in underwater optical wireless communication using deep reinforcement learning approach," in *2023 7th International Conference on I-SMAC (IoT in Social, Mobile, Analytics and Cloud) (I-SMAC)* (Piscataway, NJ: IEEE), 282–287. doi: 10.1109/I-SMAC58438.2023.10290678

Shafi, F., Kumar, A., Nakkeeran, R., and Thachayani, M. (2025). Performance analysis of underwater optical wireless communication in different ocean water types using spatial diversity. *J. Opt.* doi: 10.1007/s12596-025-02944-9. [Epub ahead of print].

Shin, H., Baek, S., and Song, Y. (2024). Multidimensional beam optimization in underwater optical wireless communication based on deep reinforcement learning. *IEEE Internet Things J.* 11, 28623–28634. doi: 10.1109/JIOT.2024.3404476

Simon, J., Kapileswar, N., and Mohanakumar, A. (2025). A novel energy adaptive neural network and deep Q-learning network for improved energy efficiency in dynamic underwater iot environment. *IEEE Access* 13, 141403–141419. doi: 10.1109/ACCESS.2025.3597025

Subramaniam, A., Wong, M. L., Borker, R. D., Nimmagadda, S., and Lele, S. K. (2020). Turbulence enrichment using physics-informed generative adversarial networks (version 2). *arXiv*. doi: 10.48550/arXiv.2003.01907

Sun, W. (2025). Generative adversarial networks (GANs): principles, development, challenges, and diverse applications. *Appl. Comput. Eng.* 165, 152–158. doi: 10.54254/2755-2721/2025.LD25482

Vali, Z., Michelson, D., Ghassemlooy, Z., and Noori, H. (2025). A survey of turbulence in underwater optical wireless communications. *Optik* . 320, 172126. doi: 10.1016/j.ijleo.2024.172126

Wang, J., and Willner, A. E. (2014). "Using orbital angular momentum modes for optical transmission," in *Optical Fiber Communication Conference* (Washington, DC: Optica Publishing Group), W4J.5. doi: 10.1364/OFC.2014.W4J.5

Wulff, M., Wang, L., Koelpin, A., and Schuster, C. (2023). "Influence of the communication environment on orbital angular momentum (OAM) mode orthogonality," in *2023 53rd European Microwave Conference (EuMC)* (Piscataway, NJ: IEEE), 786–789. doi: 10.23919/EuMC58039.2023.10290384

Ye, J., Kang, H., Cai, Q., Hu, Z., Solyanik-Gorgone, M., Wang, H., et al. (2024). Multiplexed orbital angular momentum beams demultiplexing using hybrid optical-electronic convolutional neural network. *Commun. Phys.* 7:105. doi: 10.1038/s42005-024-01571-3

Zhan, H., Wang, L., Wang, W., and Zhao, S. (2021). Experimental analysis of adaptive optics correction methods on the beam carrying orbital angular momentum mode through oceanic turbulence. *Optik* 240:166990. doi: 10.1016/j.ijleo.2021.166990

Zhang, H., Chen, C., Li, F., Cai, J., Yao, L., Dong, F., et al. (2025). Single-pass wavefront reconstruction via depth heterogeneity self-supervised neural operator for turbulence correction. *Laser Photon. Rev.* 19:e00909. doi: 10.1002/lpor.202500909

Zhang, Z., Xie, X., Si, J., Wang, W., Jia, S., and Gao, D. (2024). Turbulence compensation with pix-to-pix generative adversarial networks in vector vortex beams. *Phys. Scripta* 99:105532. doi: 10.1088/1402-4896/ad74b8